Designing two-photon molecular emitters in nanoparticle-on-mirror cavities

S. Smeets,^{1,*} B. Maes,^{1,†} G. Rosolen,^{1,‡} and C. Van Dyck^{2,§}

¹ Micro- and Nanophotonic Materials Group, Research Institute for Materials Science and Engineering, University of Mons, 20 Place du Parc, Mons B-7000, Belgium
² Theoretical Chemical Physics Group, Research Institute for Materials Science and Engineering, University of Mons, 20 Place du Parc, Mons B-7000, Belgium
(Dated: October 20, 2025)

Two-photon spontaneous emission (TPSE) is a second-order quantum process with promising applications in quantum optics that remains largely unexplored in molecular systems, which are usually very inefficient emitters. In this work, we model the first molecular two-photon emitters and establish the design rules, highlighting their differences from those governing two-photon absorbers. Using both time-dependent density functional theory and Pariser-Parr-Pople calculations, we calculate TPSE in three π -conjugated molecules and identify a dominant pathway. To overcome the inherently low TPSE rates in vacuum, we propose plasmonic nanoparticle-on-mirror cavities, engineered for degenerate TPSE. Our simulations reveal over 10 orders of magnitude enhancement and radiative efficiencies exceeding 50%. Notably, for nitro-substituted phenylene vinylene in an optimized nanocone-on-mirror structure, the two-photon emission rate surpasses that of vacuum one-photon emission from a unit dipole. These findings open new avenues for efficient and molecular-based on-demand sources of entangled photon pairs.

CONCEPTUAL INSIGHTS

This work reports, for the first time, the investigation, design and theoretical demonstration of large two-photon spontaneous emission (TPSE) from molecular systems. Unlike previous studies limited to simple atomic emitters or the extensively studied two-photon absorption counterpart, molecular TPSE is a completely unexplored concept and application for conjugated chromophores. This is largely due to the notoriously weak nature of the two-photon emission process, largely dominated by one-photon processes. To overcome the inherently weak two-photon emission rates of molecules, we engineer plasmonic nanoparticle-on-mirror cavities and demonstrate TPSE enhancement by over ten orders of magnitude. We provide spectroscopic rules to design efficient conjugated molecules for TPSE applications. In the optical cavity, carefully designed chromophores exhibit two-photon emission rates that exceed typical one-photon fluorescence rates by more than a factor of 50. This has never been anticipated elsewhere that a molecular structure may act as such an efficient two-photon emission source. This approach exceeds state-of-the-art methods for generating entangled photons such as spontaneous parametric down-conversion and four wave mixing. The molecular and nanocavity design that we propose will provide for a new platform for TPSE applications. This includes next-generation quantum light sources, with practical implications for integrated quantum photonic technologies.

I. INTRODUCTION

Two-photon spontaneous emission (TPSE) is a second-order quantum electrodynamics process in which an excited quantum emitter decays by simultaneously emitting two photons [1]. First predicted by Göppert-Mayer in 1931 [2], TPSE is typically 8 orders of magnitude weaker than single-photon emission [3], but plays a crucial role in phenomena such as the long lifetime of the hydrogen 2s state [4], which gives rise to the continuous spectrum observed from planetary nebulae [5]. TPSE has been extensively studied in various systems, including atoms [6–8], quantum dots [9, 10], semiconductors [11, 12] emitters, and also in proximity of plasmonic nanostructures [13–18].

However, TPSE remains completely unexplored in molecular systems, both theoretically and experimentally, despite their remarkable tunability enabled by chemical design [19]. Moreover, their nanoscale size makes them compatible with nanophotonic architectures and ideal for integrated quantum optical platforms [20, 21]. Given the potential of TPSE for generating on-demand entangled photons [8, 10–12], designing broadband emitters [13, 14, 22], and probing otherwise inaccessible dark states [12], understanding and tailoring TPSE in molecules is of fundamental interest for both quantum optics and molecular spectroscopy. In contrast to simple atomic emitters previously investigated [8, 15, 16], molecular systems require quantum chemistry approaches to capture their complex multielectron nature and necessitate new design principles.

Identifying bright and practical sources of entangled photons, especially operating at telecommunication wavelengths, remains a key objective for advanced quantum technologies such as secure communication, quantum computation, and teleportation [8, 11, 23]. Among the available techniques, spontaneous parametric down-

^{*} Steve.Smeets@umons.ac.be

[†] Biorn.Maes@umons.ac.be

[‡] Gilles.Rosolen@umons.ac.be

[§] Colin.VanDyck@umons.ac.be

conversion (SPDC) in non-linear crystals with secondorder optical nonlinearity is the most established approach, in which a single high-energy pump photon is converted into a pair of lower-energy and entangled photons [23, 24]. In contrast, four-wave mixing (FWM) occurs in third-order non-linear media such as optical fibers or photonic waveguides, thus particularly attractive for integrated photonic platforms, where two pump photons interact to produce the entangled photon-pair [25]. Both SPDC and FWM, however, are probabilistic processes that require phase-matching conditions, and can suffer from multi-pair generation and background noise, which limit their scalability and fidelity [8, 25]. Another approach is cascade emission, where an excited quantum emitter emits two photons sequentially via an intermediate state through two first-order transitions. Unlike SPDC and FWM, cascade emission, like TPSE, can operate deterministically and on-demand, as it involves only a single quantum emitter [10].

Among these processes, TPSE is a promising alternative. It is theoretically predicted to be up to three orders of magnitude more efficient than SPDC under equivalent pumping conditions [11], as it is a second-order process in perturbation theory, whereas SPDC is a third-order one. Moreover, TPSE offers greater spectral flexibility, as it does not require phase matching like SPDC and FWM [8], and, unlike cascade emission, does not depend on the intermediate state since it is a non-resonant process [26]. Thus, the energy of the photons emitted via TPSE can be tuned by designing the photonic environment [8]. Furthermore, TPSE is suitable for on-chip integration, enabling the design of compact and efficient entangled photon sources using for instance nanostructures coupled to waveguides [27], photonic crystals [28], or cavities [29].

Despite the lack of investigations on TPSE in molecules, two-photon absorption (TPA), the inverse process of TPSE, has been the subject of extensive study [19, 30]. In particular, π -conjugated chromophores, often incorporating donor and acceptor groups, have attracted considerable attention due to their large TPA cross-sections and the fact that one-photon transitions can be forbidden in centrosymmetric systems [19, 30]. Furthermore, numerous theoretical studies have explored the calculation of TPA using different methods, such as semi-empirical methods [31, 32] and time-dependent density functional theory (TD-DFT) [30, 33]. Therefore, the insights gained from these studies can be leveraged to calculate TPSE in molecular systems.

To overcome the inherent weakness of second-order interactions compared to first-order ones, these processes can be enhanced by shaping the electromagnetic environment surrounding the emitter [3, 34, 35]. Indeed, the spontaneous emission rate is not solely an intrinsic property of the emitter, but also depends on its photonic environment, a phenomenon known as the Purcell effect [36]. Thus, plasmonic [3, 37–40] and hybrid plasmonic-dielectric [41, 42] nanoantennas are widely em-

ployed for this purpose, as they enable nanoscale light confinement in the form of surface plasmons, thereby allowing spontaneous emission rates to be tailored. As a result, it is possible to design systems in which TPSE can outperform one-photon spontaneous emission (OPSE) [8, 34].

Among plasmonic nanoantennas, the nanoparticle-onmirror (NPoM) configuration stands out for combining a high Purcell factor and a high quantum efficiency (i.e., a high probability of emitting photons into the far field) [20, 21, 40, 43, 44]. Notably, in comparable hybrid metal-dielectric configurations, nanocones outperform nanospheres by achieving a Purcell factor up to one order of magnitude higher along with a greater quantum efficiency of 80% instead of 60% for the emission of single photons [41, 45]. Motivated by these advantages, we employ NPoM cavities to enhance two-photon emission from molecular emitters. Furthermore, we compare different nanoparticle geometries (cones, spheres, and cubes) in the context of TPSE, which is a broadband process characterized by a spectrum, in contrast to the narrowband nature of OPSE [1].

This work offers the first investigation of TPSE in molecular systems and is structured as follows. We first establish design rules for efficient two-photon molecular emitters, highlighting a key difference from those applicable to two-photon absorbers. Next, we calculate TPSE rates for three chromophores (two diphenyl polyenes and one phenylene vinylene derivative) that satisfy these criteria, employing both time-dependent density functional theory (TD-DFT) and the semi-empirical Pariser-Parr-Pople (PPP) model. We demonstrate that TPSE is primarily mediated by a bright intermediate state energetically located just above a dark initial excited state. Finally, to overcome the inherently low TPSE rates in vacuum, we design and compare different NPoM cavities. The TPSE enhancement near plasmonic structures is computed using our previously developed framework [16], originally demonstrated for a state-of-the-art hydrogenlike emitter. In the optimal configuration, we predict TPSE rates exceeding one billion per second.

II. DESIGN RULES FOR TWO-PHOTON EMITTERS

We consider a system composed of a quantum emitter (e.g., an atom, a molecule, or a quantum dot) and its photonic environment. Using the second-order Fermi's golden rule, we can show that the probability per unit time that the system (emitter plus field) performs a second-order transition from an initial state $|i\rangle$ to a final state $|f\rangle$ by emitting two quanta, upon the interaction between the emitter and the electromagnetic field, can be written as [1, 16, 26, 46, 47]:

$$\Gamma^{(2)} = \int_0^{\frac{1}{2}} \phi^{(2)}(\nu) \, \mathrm{d}\nu, \tag{1}$$

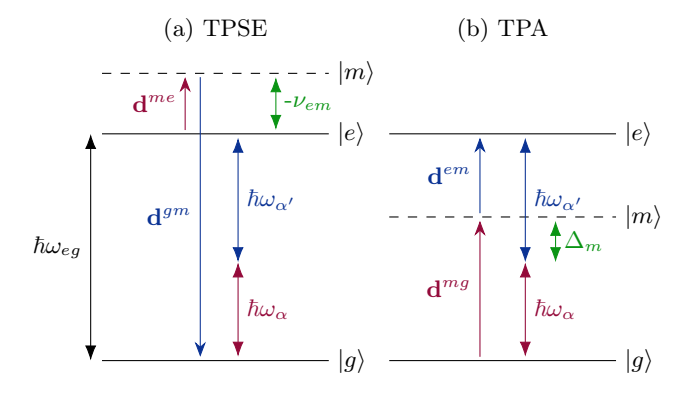


FIG. 1. Energy representation of second-order transitions [1, 26, 47]. The two photons have complementary frequencies: $\omega_{\alpha} + \omega_{\alpha'} = \omega_{eg}$. (a) Two-photon spontaneous emission (TPSE): the emitter carries-out a first transition from its excited state $|e\rangle$ to a virtual intermediate state $|m\rangle$, described by the transition moment \mathbf{d}^{me} , by emitting a first photon in the mode α . Quasi-simultaneously afterwards, a second transition described by the transition moment \mathbf{d}^{gm} is carried out to the ground state $|g\rangle$ of lower energy by emitting a second photon in the mode α' . (b) Two-photon absorption (TPA): reverse process. The emitter initially in its ground state $|q\rangle$ absorbs a first photon in the mode α to reach a virtual intermediate state $|m\rangle$, then absorbs a second photon in the mode α' to transit towards the excited state $|e\rangle$. The detuning factor Δ_m corresponds to the energy mismatch between the energy of the photon being absorbed and the energy gap between the ground and the intermediate states [19].

where $\nu := \omega/\omega_{eg}$ is the dimensionless frequency comprised between 0 and 1 and $\phi^{(2)}(\nu)$ is the decay profile. $\hbar\omega_{eg} := E_e - E_g$, with \hbar the reduced Planck constant, represents the energy gap between the excited state $|e\rangle$ and the ground state $|g\rangle$. For TPSE [Fig. 1(a)], the initial state of the system is characterised by the emitter in an excited state $|e\rangle$ and the field in the vacuum state $|vac\rangle$, while in the final one the emitter is in its ground state $|g\rangle$ and the field is in a two-quanta state. In the intermediate states that connect these two states, the emitter is in the state $|m\rangle$ and the field is in a one-quantum state. Furthermore, $\phi^{(2)}(\nu) d\nu$ denotes the number of photons emitted per second in the frequency interval between ν and $\nu + d\nu$. This definition encompasses photons emitted simultaneously at complementary frequencies (i.e., at the frequencies $1-\nu$), thus necessitating integration over only half of the spectrum in Eq. (1). Also, the probability of emitting a photon at the frequency ν is equal to the probability of emitting a photon at the complementary energy $1 - \nu$, resulting in symmetric decay profiles $\phi^{(2)}(\nu)$ with respect to $\nu = 1/2$.

When TPSE is composed of two electric dipole transitions [Fig. 1(a)], the vacuum decay profile is given by [1, 16, 26, 46, 47]:

$$\phi_0^{(2)}(\nu) = \frac{\omega_{eg}^5}{18\pi^3 \varepsilon_0^2 \hbar^2 c^6} \nu^3 (1 - \nu)^3 \| \mathcal{D}^{eg}(\nu) \|^2, \quad (2)$$

with ε_0 the vacuum electric permittivity, c the speed

of light in vacuum, and where the squared norm of the second-rank tensor is defined as $\|\mathcal{D}^{eg}\|^2 := \sum_{i,j} |\mathcal{D}^{eg}_{ij}|^2$. This equation involves the second-order electric dipole transition moment (two-photon matrix element) [1, 16, 26, 46, 47]:

$$\mathcal{D}^{eg}(\nu) := \sum_{|m\rangle} \left(\frac{\mathbf{d}^{em} \, \mathbf{d}^{mg}}{\nu_{em} - \nu} + \frac{\mathbf{d}^{mg} \, \mathbf{d}^{em}}{\nu_{em} - (1 - \nu)} \right), \quad (3)$$

where the outer product is implied and where $\nu_{em} := \omega_{em}/\omega_{eg}$, with $\hbar\omega_{em} := E_e - E_m$, with E_m the energy of the emitter in the intermediate state $|m\rangle$. Note that we chose this definition involving normalized frequencies instead of the state energies to remove the dependency with respect to ω_{eg} , facilitating subsequent comparison between different molecules. In addition, $d^{ab} := \langle a|\mathbf{d}|b\rangle$, with \mathbf{d} the electric dipole moment operator, is the electric dipole transition moment describing the transition of the emitter from the state $|b\rangle$ to the state $|a\rangle$. The tensor $\mathcal{D}^{eg}(\nu)$ involves a summation over all the intermediate states $|m\rangle$ of the emitter that connect, through the selection rules, the excited state $|e\rangle$ to the ground state $|a\rangle$.

This paper focuses on TPSE, a second-order transition, rather than on cascades of two single-photon transitions. In TPSE, the sum over states (SOS) includes only intermediate states with energies equal to or higher than that of the excited state [26, Fig. 1(a)], implying that ν_{em} in equation (2) is a negative or zero number. As a result, the law of conservation of energy is temporarily violated since during the first transition to the intermediate state, the energy of the emitter increases while a photon is emitted. The intermediate states that mediate transitions without energy conservation are called virtual states [1, 48] and their existence is limited in time by the uncertainty principle. Therefore, the two transitions in TPSE [Fig. 1(a)] are quasi-simultaneous. Another consequence is that TPSE involves only non-resonant states: the energy gap between two states is not equal to the energy of the emitted photon, avoiding denominators tending towards 0 in Eq. (3) and leading to a continuous emission spectrum [49]. In contrast, the cascade of two single-photon transition is made of two sequential firstorder processes. Moreover, in that case the SOS includes only intermediate states lying at lower energies than the initial excited state and involves only resonant states [26].

TPSE is characterised by a spectrum [Eq. (2)], which is maximum in the case of degenerate TPSE, i.e., when the two emitted photons have the same frequency $\omega = \omega_{eg}/2$ (then $\nu = 0.5$). Consequently, a higher TPSE rate is achieved by designing a structure that enhances emission at half the transition frequency. Therefore, from equations (2) and (3) we conclude that

$$\phi_0^{(2)}(\nu = 0.5) \propto \left\| \sum_{|m\rangle} \frac{\mathbf{d}^{em} \mathbf{d}^{mg}}{\nu_{em} - 0.5} \right\|^2,$$
 (4)

where, as a reminder, ν_{em} is a negative number or zero.

Therefore, TPSE scales with the transition moments to the fourth power and is inversely proportional to the square of the energy gaps between the excited state and the intermediate states. Therefore, an efficient twophoton emitter has an intermediate state $|m\rangle$ just above the two-photon excited state $|e\rangle$ (small $|\nu_{em}|$) [Fig. 1(a)], which is characterized by strong one-photon transitions between the excited and the intermediate states (high \mathbf{d}^{em}) as well as between the intermediate and the ground states (high \mathbf{d}^{mg}). Furthermore, ideally the initial excited state must be dipole forbidden, so that TPSE is the main decay path. Finally, the sum over the intermediate states indicates that several two-photon paths are possible between the excited and ground states of the emitter (i.e., multiple intermediate states connect the excited state with the ground state), there is interference between these paths, which can be constructive or destructive [17, 26].

Comparison with two-photon absorption

Regarding two-photon absorption (TPA) [Fig. 1(b)], the cross-section δ , like the TPSE rate, is proportional to the squared norm of the second-order transition moment [Eq. (3)], except that ν_{em} is replaced by $\nu_{mg} := \omega_{mg}/\omega_{eg}$ (with $\hbar\omega_{mg} := E_m - E_g$ a positive number) since it is the inverted process [1, 25]. Thus, in the case of degenerate TPA, we conclude that [19, 33]:

$$\delta \propto \left\| \sum_{|m\rangle} \frac{\mathbf{d}^{em} \mathbf{d}^{mg}}{\Delta_m} \right\|^2, \tag{5}$$

where $\Delta_m := \omega_{mg} - \frac{\omega_{eg}}{2}$ is called the detuning factor [Fig. 1(b)]. Often, the SOS is dominated by a single intermediate state, for which the detuning factor is small [19, 32]. Note that if $\Delta_m = 0$, then the energy gap between the states corresponds to the energy of the photons (resonant intermediate states) and, therefore, the cascade of two independent one-photon absorptions is the dominant absorption path [19, 26].

Given Eq. (5), a good absorber for TPA has a strong transition close to the energy of the absorbed photons (small Δ_m) [19, Fig. 1(b)]. This contrasts with the design rule established for TPSE (i.e., a strong transition just above the excited state). Therefore, molecules optimized for TPA are not good candidates for TPSE. On top of that, TPA can easily be reached by tuning the exciting laser with the energy of the excited state energy. For TPSE however, the initial state must be the first excited state for two reasons. First, if there are states lying between the excited and ground states, then a cascade of two independent one-photon transitions will dominate [26]. This can eventually be solved by designing the environment such that one-photon transitions are weaker than two-photon transitions [8]. Second, a molecule emits light predominantly from the lowest excited state due to Kasha's rule, which states that higher

excited states quickly relax to the lowest excited state due to non-radiative processes [50].

As a conclusion, a good TPSE molecular emitter can be designed according to the following rules: (1) the emission should originate from the first excited state that is dipole forbidden and (2) a small energy gap should exist between the first excited state and an intermediate state that exhibits strong transition dipole moments with both the first excited state and the ground state.

III. CALCULATION OF VACUUM TWO-PHOTON SPONTANEOUS EMISSION RATE IN MOLECULES

Having established the design rules for two-photon emitters, we now compute the vacuum two-photon spontaneous emission (TPSE) rate using quantum chemistry methods for three planar molecules that fulfil these criteria: trans-diphenylbutadiene (DPB), trans-diphenylhexatriene (DPH), and nitro-substituted benzene-1,4-bis(phenylene vinylene) (NO2-OPPV) This represents the first theoretical [Fig. 2(a,b)]. calculations of TPSE in molecular systems. molecules share key spectral characteristics [51–56]: a low-lying dark dipole forbidden excited state (thus with a one-photon transition dipole moment \mathbf{d}^{eg} close to zero), followed by a bright excited state with a large one-photon transition moment \mathbf{d}^{mg} , as well as a strong dipole coupling \mathbf{d}^{em} with the dark excited state and a small energy gap $|\nu_{em}|$ between them.

In the geometry of their first excited state (from which two-photon emission occurs), the three molecules transform under the C_{2h} point group [57]. A schematic representation of the allowed electric dipole transitions between the symmetries is shown in Fig. 2(c). For this point group, the most favourable situation arises when the first excited state has the same symmetry as the ground state, namely A_g , which is the case for the three considered molecules. In this configuration, one-photon transitions are dipole forbidden (dark state), and two TPSE paths are dipole-allowed by symmetry: $2A_g \xrightarrow{xy} B_u \xrightarrow{xy} 1A_g$ and $2A_g \xrightarrow{z} A_u \xrightarrow{z} 1A_g$.

For all three molecules under study, the two lowest excited states are $2A_g$ (dark) and $1B_u$ (bright), respectively [51–56]. Moreover, the transition dipole moments are predominantly oriented along the molecular axis [58], i.e., the x direction in Figure 2(a,b). As a result, the TPSE process is dominated by the path using B_u intermediate sates over A_u intermediate states [Fig. 2(d)]. Moreover, only the xx component of the second-order transition moment \mathcal{D}^{eg} [Eq. (3)] is non-zero. Although multiple B_u intermediate states connect the initial and the ground states, the lowest one, $1B_u$, is expected to contribute the most due to a small energy gap $|\nu_{em}|$ [Eq. (4)]. Note that although transitions from triplet excited states to the singlet ground state (phosphorescence) are in principle possible, they are spin-forbidden. They are there-

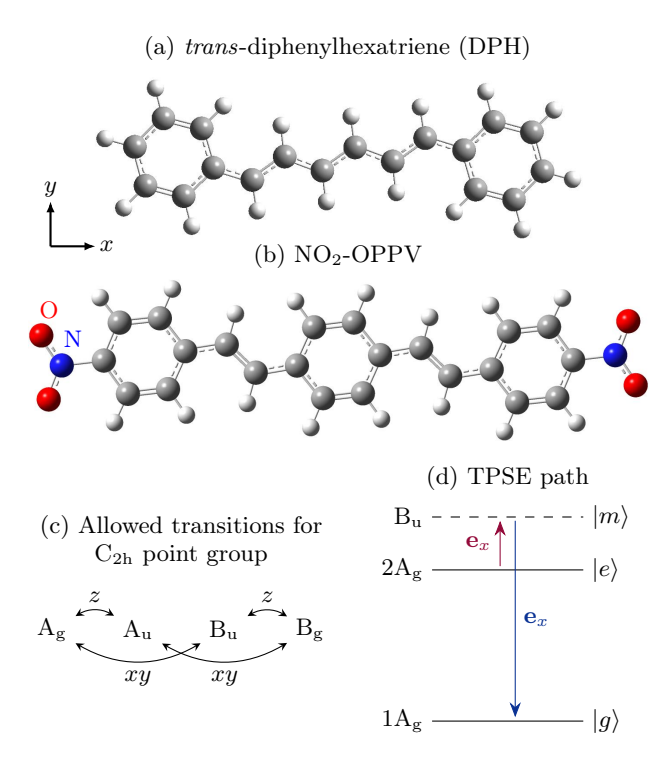


FIG. 2. (a, b) Molecular structures visualised using GaussView 6. trans-diphenylbutadiene (DPB, not shown) is structurally similar to DPH, but the two phenyl groups are connected by a four-carbon polyene chain instead of a six-carbon one. (c) Allowed electric dipole transitions for the C_{2h} point group [57]. (d) Representation of the dominant TPSE path for the three studied molecules.

fore negligible in the studied systems, which are composed of light atoms where spin–orbit coupling is weak.

A. Method

To evaluate vacuum TPSE rates [Eq. (2)], it is necessary to compute the excitation energies along with the transition dipole moments \mathbf{d}^{mg} and \mathbf{d}^{em} , which describe, respectively, the transitions between the ground and excited states, and between pairs of excited states. These quantities are required to construct the sum-overstates (SOS) expression [Eq. (3)] that governs second-order processes. They are calculated in this study using the quadratic response double residue (QRDR) formalism within time-dependent density functional theory (TD-DFT) [30, 33], as implemented in Dalton 2020.1 quantum chemistry software [59, 60].

Reliable predictions of second-order properties using DFT can be achieved by employing hybrid functionals and carefully truncating the SOS expansion once all relevant low-lying excited states are included (below the ionisation threshold), while excluding poorly described Rydberg and continuum states [30, 33]. Accordingly, we compare three TD-DFT theory levels for computing the $2A_{\rm g}$ and the 7 lowest $B_{\rm u}$ excited states [30, 33]:

 $\rm B3LYP/6-31G^*,~CAM\text{-}B3LYP/6-31G^*,~and~CAM\text{-}B3LYP/6-31+G^*,~the latter being more appropriate for excited states [61–63]. Geometries are optimised in the <math display="inline">\rm 2A_g$ initial state at the CAM-B3LYP/6-31G* level for all three methods, using Gaussian 16 quantum chemistry software [64]. Although other functionals such as LC-B3LYP, $\omega B97X,~or~M06\text{-}2X$ are also commonly used for excited state calculations [61–63], they are not available in Dalton. Nevertheless, our approach provides correct orders of magnitude and robust qualitative trends, which is sufficient for a proof-of-concept study focused on fundamental feasibility and design principles.

TD-DFT methods are known, from both theoretical and experimental studies [33, 51, 65–67], to inaccurately describe excited states with large double-excitation character, such as the A_g states in π -conjugated molecules. As a result, these methods incorrectly predict that the $1B_u$ state lies below the $2A_g$ state for the three molecules under consideration [51–56]. In this situation, the calculation of TPSE from the $2A_g$ state does not include the contribution of the $1B_u$ intermediate state since the SOS series only include terms above the initial state [26], whereas it is expected to dominate due to a small value of $|\nu_{em}|$ [Eq. (4)]. In addition, transition moments tend to be overestimated [68], typically by 20 to 150% for second-order properties [33, 52, 53, 56].

To address the TD-DFT limitation, we employ configuration interaction (CI) within the Pariser-Parr-Pople (PPP) semiempirical model [69], including both single and double excitations, to calculate the energy gap ΔE_{21} between the 2A_g and 1B_u states. These calculations are performed using the ZINDO package [70], based on geometries optimized via TD-DFT. Indeed, the PPP model, which considers only π -electrons [69], is well suited for describing the electronic structure of planar conjugated molecules, like diphenylpolyenes and phenylene-vinylene oligomers [31, 51, 56]. Therefore, the PPP computed energy gap is used to correct the TD-DFT results: the 2A_g state is manually shifted below the $1B_u$ state such that the energy gap ΔE_{21} between them is the same as calculated with the PPP model. Note that we did not modify the energy of the intermediate states, since B_n states are well described with TD-DFT methods [33, 51, 65–67]. Transition dipole moments calculated using TD-DFT and PPP are reported in Supplementary Information for comparison.

B. Results

The results at the CAM-B3LYP/6 – 31+G* level for the three molecules are presented in Table I and in Figure 3. First, PPP calculations accurately capture the energy gap between the $2A_{\rm g}$ and $1B_{\rm u}$ states. In contrast, TD-DFT energies deviate by up to 0.65 eV from experiment [Tab. I], even when corrected by PPP. As a result, TPSE rates are underestimated for DPB and DPH, but overestimated for NO₂-OPPV, as they scale with the fifth

power of the transition energy [Eq. (2)]. Second, the vacuum TPSE rate of DPH exceeds that of DPB [Fig. 3(a)] due to larger transition moments d^{12} and d^{20} , despite its smaller transition frequency and larger energy gap ΔE_{21} . Third, the TPSE rate of NO₂-OPPV is higher than that of DPH, owing to a smaller energy gap ΔE_{21} and to larger transition moments d^{12} and d^{20} . Note that using experimental values for ΔE_{10} to calculate TPSE rates [Eq. (2)], the TPSE rate of NO₂-OPPV remains greater than that of DPH, by 12%. Overall, the integrated vacuum TPSE rates range from 2.82×10^{-2} (DPB) to 8.54×10^{-1} s⁻¹ (NO₂-OPPV). For comparison, the integrated vacuum TPSE rate for the $2s \rightarrow 1s$ transition in hydrogen is 8.23 s⁻¹ [5], an order of magnitude higher.

Results obtained with three TD-DFT theory levels $(B3LYP/6-31G^*, CAM-B3LYP/6-31G^*, and CAM-B3LYP/6-31+G^*)$ are reported in Supporting Information. The calculated rates differ by at most a factor of 3.3, so the conclusions remain unchanged regardless of the method used. Additionally, the transition moments calculated with the PPP model are also reported in Supporting Information. They are larger than those computed from TD-DFT, leading to \mathcal{D}^{eg} values that are 9.7, 2.1, and 2.6 times higher for DPB, DPH, and NO₂-OPPV molecules, respectively. This alternative method would then predict TPSE rates that are larger by up to two orders of magnitude.

Concerning the number of states included in the SOS, the convergence of \mathcal{D}^{eg} is plotted in Figure 3b. The relative deviation obtained by including only the first intermediate state $1B_u$ ranges from +3% to +30% compared to the reference value computed with the first seven B_u states. This highlights that $1B_u$ dominates the contribution, but also slightly overestimates the total. This dominant contribution arises not only from a smaller value of ν_{em} , but also from stronger coupling with the excited state $2A_g$. Moreover, the relative contribution of each intermediate state decreases progressively with increasing energy. Finally, the convergences exhibit both constructive and destructive interference effects, i.e., inclusion of higher energy states may either contribute positively or negatively.

IV. ENHANCEMENT WITH A PLASMONIC NANOANTENNA

We now design a plasmonic nanocavity to enhance two-photon emission into the far field. To achieve this, we consider NPoM structures due to their ability to enhance emission while maintaining a high quantum efficiency [41, 45]. To compute the TPSE enhancement, we employ our previously developed framework [16], originally demonstrated for a state-of-the-art hydrogen-like emitter. The method is detailed in the next subsection. We describe here the most efficient structure, namely a truncated gold nanocone placed above a flat gold mirror [40, 41, Fig. 4], and we finally compare it with other

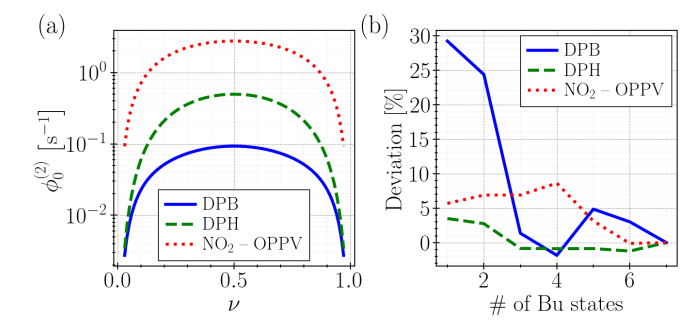


FIG. 3. (a) Two-photon spontaneous emission rates in vacuum. (b) Convergence of the norm of \mathcal{D}^{eg} at $\nu=0.5$ [Eq. (3)] as a function of the number of B_u states included in the SOS. The values represent the relative deviation with respect to the reference value computed using the first seven B_u states.

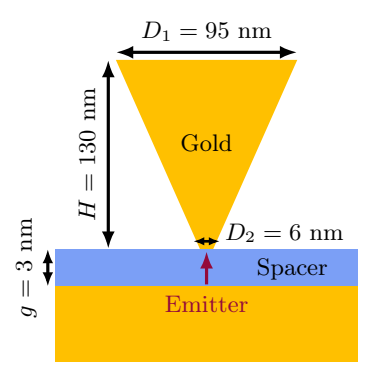


FIG. 4. Cross-sectional view of the three-dimensional nanoantenna, consisting of a nanoparticle-on-mirror (NPoM) cavity. The molecule is placed vertical inside the gap (red vertical arrow). Geometric parameters are reported for the structure optimised for the NO_2 -OPPV molecule [Tab. II].

particle geometries (sphere and cubes). The gap is filled with a dielectric spacer embedding the emitter positioned in the middle of the gap and which is oriented vertically (long molecular axis), so that its electric dipole transition moment is along the local electric field [20, 71, 72] (red arrow in Fig. 4).

The gold nanocone finishes with a flattened tip end of 3 nm radius [41, 45]. In addition, the spacer gap size is set to be approximately one nanometer thicker than the length of the molecules: gap sizes of 2.5 nm for DPB and DPH, and of 3.0 nm for NO₂-OPPV. This design preserves stable field enhancement, prevents molecular aggregation with the structure, ensures optimal alignment of the transition dipole moment along the cone axis, limits charge transfer and chemical reactions with the metal surfaces, and enables the insertion of the spacer [20, 71, 72]. Furthermore, we set the refractive index of the spacer to n = 1.4, which corresponds, for instance, to that of macrocyclic cucurbit[n]uril molecules, commonly used as host-guest platforms in plasmonic nanocavities [20, 71, 72]. Although this parameter could also be optimised, the rate enhancement is predominantly determined by the metallic com-

Molecule	$\Delta E_{10} \text{ [eV]}$	$\Delta E_{21} \text{ [eV]}$	d^{12} [a.u.]	d^{20} [a.u.]	$\mathcal{D}^{eg}(0.5)$ [a.u.]	$\phi_0^{(2)}(0.5) [s^{-1}]$	$\Gamma_0^{(2)} \left[s^{-1} \right]$
DPB	3.43 (3.67 [52, 53])	0.17 (0.14 [52, 53])	0.91	4.16	10.3	9.30×10^{-2}	2.82×10^{-2}
DPH	2.55 (3.19 [54, 55])	0.40 (0.42 [54, 55])	3.16	5.38	49.8	4.96×10^{-1}	1.34×10^{-1}
NO_2 -OPPV	2.92 (2.58 [56])	0.10	4.29	5.51	83.8	2.76	8.54×10^{-1}

TABLE I. Optical emission properties of the TPSE molecular emitters. TD-DFT results using CAM-B3LYP/6-31+G* (geometry optimized with CAM-B3LYP/6-31G*), where the energy gap ΔE_{21} is calculated using the PPP model and used to correct the energy of the $2A_g$ state (first excited state). ΔE_{10} and ΔE_{21} are, respectively, the energy gaps between the first excited state ($2A_g$) and the ground state ($1A_g$), between the second excited state ($1B_u$) and the first excited state ($2A_g$). Experimental values are indicated in parentheses. d^{12} and d^{20} represent the norm of the electric dipole transition between the first and second excited states, and between the second excited state and the ground state. $\mathcal{D}^{eg}(0.5)$ is the norm of the second-order transition moment [Eq. (3)] for $\nu = 0.5$ and a TPSE transition from first excited state ($2A_g$) to the ground state ($1A_g$). $\phi_0^{(2)}$ and $\Gamma_0^{(2)}$ are, respectively, the vacuum spectral TPSE rate at $\nu = 0.5$ and the integrated vacuum TPSE rate [Eq. (1)].

ponent of the structure [21, 42].

A. Method

For emitters whose second-order transition is dominated by a single component, specifically the xx component for the studied molecules, the two-photon Purcell effect is given by the product of two one-photon Purcell factors, one for each quantum emitted at complementary frequencies [16, 46, 47]:

$$\frac{\phi^{(2)}(\nu; \mathbf{R})}{\phi_0^{(2)}(\nu)} = P_x(\nu; \mathbf{R}) P_x(1 - \nu; \mathbf{R}), \tag{6}$$

with \mathbf{R} the emitter position (centre of its charge distribution). In this equation, $\phi^{(2)}(\nu; \mathbf{R})$ and $\phi_0^{(2)}(\nu)$ denote, respectively, the spectral distribution rate of the emitted quanta in the presence of the photonic structure and in vacuum. Moreover, P_x is the one-photon Purcell factor related to an emitter having its transition moment along the x axis (red arrow in Fig. 4). It can be computed classically by modelling electric dipole point sources in electromagnetic simulations: $P_x = W_x/W_0$ with W_x and W_0 being the powers emitted by a dipole oscillating along the x axis in the presence of the plasmonic nanocavity and in vacuum [36].

Near plasmonic structures, the two-quanta emission is mainly given by three distinct emission pathways: the photon-photon (ph-ph), photon-plasmon (ph-pl), and plasmon-plasmon (pl-pl) channels [15]. These pathways can be calculated via the decomposition of the Purcell factors into radiative and non-radiative parts: $P = P_{\rm rad} + P_{\rm n-rad}$ [15, 36, 47]. In addition, we define the TPSE quantum efficiency as the probability that the emitter decays by emitting a photon pair in the far field. Thus, it is the ratio between the integrated two-photon emission rate and the integrated total two-quanta emission

rate [18]:

$$\eta^{(2)} := \frac{\Gamma_{\text{ph-ph}}^{(2)}}{\Gamma_{\text{tot}}^{(2)}} = \frac{\int_0^{\frac{1}{2}} \phi_{\text{ph-ph}}^{(2)}(\nu) \, d\nu}{\int_0^{\frac{1}{2}} \phi_{\text{tot}}^{(2)}(\nu) \, d\nu}.$$
 (7)

Specifically, we use the COMSOL Multiphysics® software [73] based on the finite element method to compute the Purcell factors over a range of frequencies [47]. Once calculated, TPSE spectra are obtained via equation (6), with rates in vacuum having been calculated in Sec III. The simulation parameters are detailed in Section III of the Supplementary Information.

B. Results

For each molecule, the height H and the diameter D_1 of the largest base of the truncated nanocone are optimised to enhance the emission at half the transition frequency, i.e., at $\nu=0.5$. Indeed, at this frequency the vacuum TPSE rate is maximum [Eq. (2)] and the two-photon Purcell effect is the highest, as both photons have the same energy and benefit from the enhancement [15, 16]. The optimised geometric parameters as well as key TPSE-related quantities are reported for the three molecules in Table II. In addition, the Purcell factor P_x and TPSE spectra are plotted in Figure 5 for the best configuration, which corresponds to the system using the NO₂-OPPV emitter.

First, an enhancement of 10 orders of magnitude is achieved for the emission of two photons of same energy into the far field (see the $\phi_{\rm ph-ph}^{(2)}(0.5)/\phi_0^{(2)}(0.5)$ column of Table II), using the geometry parameters optimised for each molecule. The enhancement is stronger for lower transitions frequencies (see DPB and DPH lines; this is an effect of the gold material) and increases with a smaller gap. The integrated two-photon emission rates $\Gamma_{\rm ph-ph}^{(2)}$ range from $3.78\times 10^7~{\rm s}^{-1}$ for DPB to $1.41\times 10^9~{\rm s}^{-1}$ for NO₂-OPPV. Overall, NO₂-OPPV performs best due to its intrinsically higher vacuum TPSE rate [Tab. I],

Emitter	$\hbar\omega_{eg}$ [eV]	gap [nm]	D_1 [nm]	H [nm]	$\phi_{\text{ph-ph}}^{(2)}(0.5)/\phi_0^{(2)}(0.5)$	$\phi_{\rm ph-ph}^{(2)}(0.5) [{\rm s}^{-1}]$	$\Gamma_{\rm ph\text{-}ph}^{(2)}\left[s^{-1}\right]$	$\eta^{(2)}$	ξ
DPB	3.43	2.5	100	95	1.15×10^{10}	1.07×10^{9}	3.78×10^7	30.6%	0.88
DPH	2.55	2.5	115	185	3.63×10^{10}	1.80×10^{10}	8.92×10^{8}	51.9%	50.6
NO_2 -OPPV	2.92	3.0	95	130	1.69×10^{10}	4.67×10^{10}	1.41×10^{9}	40.5%	53.3

TABLE II. **Two-photon enhancement in the NPoM cavity.** The quantity $\phi_{\rm ph-ph}^{(2)}(0.5)/\phi_0^{(2)}(0.5)$ denotes the enhancement of the two-photon emission rate into the far field compared to vacuum, evaluated at $\nu=0.5$. $\Gamma_{\rm ph-ph}^{(2)}$ corresponds to the integrated two-photon emission rate [Eq. (1)]. $\eta^{(2)}$ is the quantum efficiency, defined as the probability of emitting a photon pair into the far field [Eq. (7)]. $\xi:=\Gamma_{\rm ph-ph}^{(2)}/\Gamma_0^{(1)}$, with $\Gamma_0^{(1)}=\omega_{eg}^3\|\mathbf{d}^{eg}\|^2/3\pi\varepsilon_0\hbar c^3$ [1], quantifies the enhancement of the two-photon emission rate with respect to the vacuum one-photon emission rate of an emitter with a transition dipole moment \mathbf{d}^{eg} of one atomic unit.

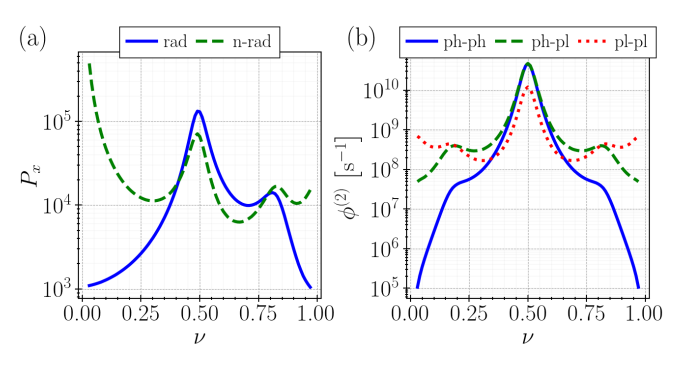


FIG. 5. Strong two-photon rate enhancement for the NO₂-OPPV molecule. (a) Radiative (rad) and non-radiative (n-rad) parts of the Purcell factor P_x . (b) Ph-ph, ph-pl, and pl-pl emission channels of the spectral TPSE rate. The quanta are emitted at the complementary frequencies ν and $1 - \nu$, leading to symmetric spectra with respect to $\nu = 0.5$.

but DPH exhibits the best quantum efficiency $\eta^{(2)}$. Compared to the one-photon emission in vacuum of a dipole emitter with a transition dipole moment of 1 atomic unit (see ξ in the last column of Table II), the far-field TPSE rates $\Gamma^{(2)}_{\rm ph-ph}$ of DPH and NO₂-OPPV are 50 times larger. This is significant as one atomic unit transition dipole moments are typical for fluorescent molecules in solution [64]. Moreover, photon emission predominantly occurs at mid-frequency, with 66% of photon pairs emitted within the full width at half maximum (spectral bandwidth $\Delta \nu = 7\%$) of the peak centred at $\nu = 0.5$ for the NO₂-OPPV emitter [Fig. 5(b)].

In Section IV of the Supplementary Information, we compare various plasmonic nanocavities for the NO₂-OPPV molecule to demonstrate that the studied structure offers the optimal enhancement and quantum efficiency. A summary of the key results is provided here. First, reducing the tip width from 6 nm to 4 nm increases the TPSE rate by 55%, but the fabrication of such a small tip is challenging [74]. Second, for the nanocone-on-mirror structure (with $D_2 = 6$ nm), the enhancement is 170-fold, 250-fold, and 75-fold higher compared to the cube-on-mirror, sphere-on-mirror, and nanocone without mirror configurations, respectively. Correspondingly, the

quantum efficiency of the nanocone-on-mirror is better by 36.7%, 28.8%, and 2.5%.

Finally, we can estimate an upper bound for the one-photon transition dipole moment of the initial excited state that ensures a decay probability greater than 90% via the TPSE process and not through the one-photon spontaneous process, i.e., $\Gamma_{\rm ph-ph}^{(2)} = 9\,P_x(\omega_{eg})\,\Gamma_0^{(1)}$. Based on the data relative to the NO₂-OPPV molecule in the nanocone-on-mirror cavity (see Table II for the integrated TPSE rate $\Gamma_{\rm ph-ph}^{(2)}$ and Figure 5(a) for the Purcell factor $P_x(\omega_{eg})$), this condition imposes a maximum one-photon emission rate in vacuum of $8.7\times10^4~{\rm s}^{-1}$, corresponding to a maximum transition dipole moment of 1.8×10^{-2} a.u. This ensures that consideration of one-photon processes, such as vibronic coupling, would not affect the conclusion of our study.

V. CONCLUSION

This work provides the first theoretical framework and quantitative predictions for two-photon spontaneous emission (TPSE) in molecular systems, extending beyond simple atomic models to complex multi-electron chromophores and establishing the foundation for molecular quantum optics applications. We demonstrate how molecular design and photonic nanostructures can be leveraged to achieve TPSE rates that surpass free-space one-photon spontaneous emission. Central to this success is the recognition that the design rules for efficient two-photon emitters differ from those for two-photon absorbers. TPSE requires an intermediate state just above the initial excited state, with strong transition dipole couplings to both the initial excited and the ground states. Additionally, while TPA can target higher-lying excited states by tuning the excitation energy, TPSE is constrained to originate from the lowest excited state due to Kasha's rule, which is ideally dipole forbidden to avoid one-photon emission. Building on these insights, we selected three π -conjugated molecules and confirmed their good TPSE performances through both the quadratic response double residue (QRDR) formalism within timedependent density functional (TD-DFT) theory and the Pariser-Parr-Pople model calculations. This study represents an initial step, where we considered single emitters, rather than an exhaustive screening. Other candidate molecules may still be discovered or chemically optimized, such as dimers or larger aggregates, where intermolecular interactions could introduce additional degrees of freedom in emitter design.

The emission from the three molecules was then dramatically enhanced using nanoparticle-on-mirror cavities, with nanocone geometries achieving up to ten orders of magnitude enhancement and radiative efficiencies exceeding 50%. Remarkably, the best configuration featuring the NO₂-OPPV molecule emits photon pairs at rates exceeding one billion par second, over 50-fold higher than the one-photon emission rate of a unit dipole in vacuum. By comparison, this rate is three orders of magnitude higher than those achieved through SPDC and FWM [75], and comparable to the rates obtained via cascade emission [76]. Other nanophotonic structures are also possible, including designs that enable integrated sources via coupling to waveguides [27].

A key perspective of this work is to provide theoretical predictions that can guide future experimental efforts and enable benchmarking of our computational methods once experimental data become available. These findings open new avenues for molecular quantum optics with a proposed system that is experimentally feasible [41, 43]. This represents a significant step toward realizing efficient, on-demand sources of entangled photon pairs based on single emitters, suitable for on-chip integration [10]. Compared to other approaches for generating entangled photon pairs, TPSE offers great tunability, making it a promising alternative for quantum photonic technologies.

AUTHOR CONTRIBUTIONS

All authors (S. Smeets, B. Maes, G. Rosolen, and C. Van Dyck) designed the research, S. Smeets performed

it, and all authors analysed the data. The first draft of the manuscript was written by S. Smeets and all authors commented, revised and approved on the final manuscript.

CONFLICTS OF INTEREST

There are no conflicts to declare.

DATA AVAILABILITY

Data for this article are available at Open Science Framework at doi.org/10.17605/OSF.IO/ZGQTB. This includes molecular geometries, computational inputs and ouputs, home-made post-processing scripts, ZINDO computational package, and COMSOL models.

The computational tools used to produce the scientific data are documented in the main text with appropriate citation of their authors. COMSOL is a commercially available software (comsol.com). Dalton is openly available (daltonprogram.org). ZINDO package is available in the provided repository.

ACKNOWLEDGMENTS

We acknowledge support from Action de Recherche Concertée (Project ARC-21/25 UMONS2) and from Vincent Lemaur (Laboratory for Chemistry of Novel Materials, University of Mons, Belgium) for assistance with the ZINDO package.

^[1] D. P. Craig and T. Thirunamachandran, *Molecular quantum electrodynamics: an introduction to radiation-molecule interactions* (Academic Press, London; Orlando, 1984).

^[2] M. Göppert-Mayer, Über elementarakte mit zwei quantensprüngen, Annalen der Physik 401, 273 (1931).

^[3] N. Rivera, I. Kaminer, B. Zhen, J. D. Joannopoulos, and M. Soljačić, Shrinking light to allow forbidden transitions on the atomic scale, Science 353, 263 (2016).

^[4] G. Breit and E. Teller, Metastability of hydrogen and helium levels., The Astrophysical Journal 91, 215 (1940).

^[5] L. J. Spitzer and J. L. Greenstein, Continuous emission from planetary nebulae, The Astrophysical Journal 114, 407 (1951).

^[6] M. Lipeles, R. Novick, and N. Tolk, Direct detection of two-photon emission from the metastable state of singly ionized helium, Physical Review Letters 15, 690 (1965).

^[7] C. L. Cesar, D. G. Fried, T. C. Killian, A. D. Polcyn, J. C. Sandberg, I. A. Yu, T. J. Greytak, D. Kleppner, and J. M. Doyle, Two-photon spectroscopy of trapped atomic hydrogen, Physical Review Letters 77, 255 (1996).

^[8] S. Ghosh, N. Rivera, G. Eisenstein, and I. Kaminer, Creating heralded hyper-entangled photons using Rydberg atoms, Light: Science & Applications 10, 100 (2021).

^[9] Y. Ota, S. Iwamoto, N. Kumagai, and Y. Arakawa, Spontaneous two-photon emission from a single quantum dot, Physical Review Letters 107, 233602 (2011).

^[10] S. Liu, Y. Wang, Y. Saleem, X. Li, H. Liu, C.-A. Yang, J. Yang, H. Ni, Z. Niu, Y. Meng, X. Hu, Y. Yu, X. Wang, M. Cygorek, and J. Liu, Quantum correlations of spontaneous two-photon emission from a quantum dot, Nature 643, 1234 (2025).

^[11] A. Hayat, P. Ginzburg, and M. Orenstein, High-rate entanglement source via two-photon emission from semi-

- conductor quantum wells, Physical Review B **76**, 035339 (2007).
- [12] A. Hayat, P. Ginzburg, and M. Orenstein, Entangled photon spectroscopy and communications based on semiconductor two-photon process, in *International Confer*ence on Quantum Information (OSA, Rochester, New York, 2007) p. JWC63.
- [13] A. Nevet, N. Berkovitch, A. Hayat, P. Ginzburg, S. Ginzach, O. Sorias, and M. Orenstein, Plasmonic nanoantennas for broad-band enhancement of two-photon emission from semiconductors, Nano Letters 10, 1848 (2010).
- [14] A. N. Poddubny, P. Ginzburg, P. A. Belov, A. V. Zayats, and Y. S. Kivshar, Tailoring and enhancing spontaneous two-photon emission using resonant plasmonic nanostructures, Physical Review A 86, 033826 (2012).
- [15] Y. Muniz, A. Manjavacas, C. Farina, D. A. R. Dalvit, and W. J. M. Kort-Kamp, Two-photon spontaneous emission in atomically thin plasmonic nanostructures, Physical Review Letters 125, 033601 (2020).
- [16] S. Smeets, B. Maes, and G. Rosolen, General framework for two-photon spontaneous emission near plasmonic nanostructures, Physical Review A 107, 063516 (2023).
- [17] S. Smeets, B. Maes, and G. Rosolen, Interference between multipolar two-photon transitions in quantum emitters near plasmonic nanostructures, Discover Nano 19, 155 (2024).
- [18] S. Smeets, B. Maes, and G. Rosolen, Tailoring directivity of two-photon spontaneous emission using plasmonic nanoantennas, Optics Letters 50, 1845 (2025).
- [19] M. Pawlicki, H. A. Collins, R. G. Denning, and H. L. Anderson, Two-photon absorption and the design of twophoton dyes, Angewandte Chemie International Edition 48, 3244 (2009).
- [20] R. Chikkaraddy, B. De Nijs, F. Benz, S. J. Barrow, O. A. Scherman, E. Rosta, A. Demetriadou, P. Fox, O. Hess, and J. J. Baumberg, Single-molecule strong coupling at room temperature in plasmonic nanocavities, Nature 535, 127 (2016).
- [21] A. I. Barreda, M. Zapata-Herrera, I. M. Palstra, L. Mercadé, J. Aizpurua, A. F. Koenderink, and A. Martínez, Hybrid photonic-plasmonic cavities based on the nanoparticle-on-a-mirror configuration, Photonics Research 9, 2398 (2021).
- [22] A. Hayat, A. Nevet, P. Ginzburg, and M. Orenstein, Applications of two-photon processes in semiconductor photonic devices: invited review, Semiconductor Science and Technology 26, 083001 (2011).
- [23] C. Couteau, Spontaneous parametric down-conversion, Contemporary Physics 59, 291 (2018).
- [24] P. G. Kwiat, K. Mattle, H. Weinfurter, A. Zeilinger, A. V. Sergienko, and Y. Shih, New high-intensity source of polarization-entangled photon pairs, Physical Review Letters 75, 4337 (1995).
- [25] R. W. Boyd, *Nonlinear optics*, 2nd ed. (Academic press, San Diego, 2003).
- [26] J. Chluba and R. A. Sunyaev, Two-photon transitions in hydrogen and cosmological recombination, Astronomy & Astrophysics 480, 629 (2008).
- [27] G. P. Agrawal, Nonlinear fiber optics, 4th ed., Quantum electronics-principles and applications (Elsevier / Academic Press, Amsterdam; Boston, 2007).
- [28] Y. Zeng, Y. Fu, X. Chen, W. Lu, and H. Ågren, Highly efficient generation of entangled photon pair by sponta-

- neous parametric downconversion in defective photonic crystals, Journal of the Optical Society of America B **24**, 1365 (2007).
- [29] A. Dousse, J. Suffczyński, A. Beveratos, O. Krebs, A. Lemaître, I. Sagnes, J. Bloch, P. Voisin, and P. Senellart, Ultrabright source of entangled photon pairs, Nature 466, 217 (2010).
- [30] K. Ohta, S. Yamada, K. Kamada, A. D. Slepkov, F. A. Hegmann, R. R. Tykwinski, L. D. Shirtcliff, M. M. Haley, P. Sałek, F. Gel'mukhanov, and H. Ågren, Two-photon absorption properties of two-dimensional π-conjugated chromophores: Combined experimental and theoretical study, The Journal of Physical Chemistry A 115, 105 (2011).
- [31] P. Tavan and K. Schulten, The low-lying electronic excitations in long polyenes: A PPP-MRD-CI study, The Journal of Chemical Physics 85, 6602 (1986).
- [32] X.-B. Zhang, J.-K. Feng, A.-M. Ren, and C.-C. Sun, Theoretical study of two-photon absorption properties of a series of ferrocene-based chromophores, The Journal of Physical Chemistry A 110, 12222 (2006).
- [33] I. H. Nayyar, A. E. Masunov, and S. Tretiak, Comparison of TD-DFT methods for the calculation of two-photon absorption spectra of oligophenylvinylenes, The Journal of Physical Chemistry C 117, 18170 (2013).
- [34] N. Rivera, G. Rosolen, J. D. Joannopoulos, I. Kaminer, and M. Soljačić, Making two-photon processes dominate one-photon processes using mid-IR phonon polaritons, Proceedings of the National Academy of Sciences 114, 13607 (2017).
- [35] N. Rivera and I. Kaminer, Light-matter interactions with photonic quasiparticles, Nature Reviews Physics 2, 538 (2020).
- [36] L. Novotny and B. Hecht, *Principles of Nano-Optics*, 2nd ed. (Cambridge University Press, Cambridge, 2012).
- [37] M. L. Andersen, S. Stobbe, A. S. Sørensen, and P. Lodahl, Strongly modified plasmon-matter interaction with mesoscopic quantum emitters, Nature Physics 7, 215 (2011).
- [38] A. M. Kern and O. J. F. Martin, Strong enhancement of forbidden atomic transitions using plasmonic nanostructures, Physical Review A 85, 022501 (2012).
- [39] G. Rosolen and B. Maes, Strong multipolar transition enhancement with graphene nanoislands, APL Photonics 6, 086103 (2021).
- [40] F. Marquier, C. Sauvan, and J.-J. Greffet, Revisiting quantum optics with surface plasmons and plasmonic resonators, ACS Photonics 4, 2091 (2017).
- [41] X.-W. Chen, M. Agio, and V. Sandoghdar, Metallodielectric hybrid antennas for ultrastrong enhancement of spontaneous emission, Physical Review Letters 108, 233001 (2012).
- [42] A. Barreda, S. Hell, M. Weissflog, A. Minovich, T. Pertsch, and I. Staude, Metal, dielectric and hybrid nanoantennas for enhancing the emission of single quantum dots: A comparative study, Journal of Quantitative Spectroscopy and Radiative Transfer 276, 107900 (2021).
- [43] R. Chikkaraddy, X. Zheng, F. Benz, L. J. Brooks, B. De Nijs, C. Carnegie, M.-E. Kleemann, J. Mertens, R. W. Bowman, G. A. E. Vandenbosch, V. V. Moshchalkov, and J. J. Baumberg, How ultranarrow gap symmetries control plasmonic nanocavity modes: From cubes to spheres in the nanoparticle-on-mirror, ACS Photonics 4, 469 (2017).

- [44] J. J. Baumberg, Picocavities: a primer, Nano Letters 22, 5859 (2022).
- [45] A. Mohammadi, F. Kaminski, V. Sandoghdar, and M. Agio, Fluorescence enhancement with the optical (bi-) conical antenna, The Journal of Physical Chemistry C 114, 7372 (2010).
- [46] Y. Muniz, F. S. S. da Rosa, C. Farina, D. Szilard, and W. J. M. Kort-Kamp, Quantum two-photon emission in a photonic cavity, Physical Review A 100, 023818 (2019).
- [47] S. Smeets, Analytical and numerical investigation of the two-photon spontaneous emission process near plasmonic nanostructures, Ph.D. thesis, University of Mons, Belgium (2024).
- [48] P. W. Milonni, The quantum vacuum: an introduction to quantum electrodynamics (Academic Press, Boston, 1994).
- [49] V. B. Beresteckij, E. M. Lifšic, and L. P. Pitaevskij, Quantum electrodynamics, 2nd ed., Course of theoretical physics No. 4 (Butterworth-Heinemann, Oxford, 2008).
- [50] N. J. Turro, V. Ramamurthy, and J. C. Scaiano, Principles of molecular photochemistry: an introduction (University science books, Sausalito (Calif.), 2009).
- [51] M. T. Allen and D. G. Whitten, The photophysics and photochemistry of α,ω-diphenylpolyene singlet states, Chemical Reviews 89, 1691 (1989).
- [52] L. A. Heimbrook, B. E. Kohler, and T. A. Spiglanin, Free jet excitation and emission spectra of diphenylbutadiene, Proceedings of the National Academy of Sciences 80, 4580 (1983).
- [53] J. Shepanski, B. Keelan, and A. Zewail, Diphenylbutadiene in supersonic jets: Spectroscopy and picosecond dynamics, Chemical Physics Letters 103, 9 (1983).
- [54] B. E. Kohler and T. A. Spiglanin, Structure and dynamics of excited singlet states of isolated diphenylhexatriene, The Journal of Chemical Physics 80, 5465 (1984).
- [55] B. E. Kohler and T. A. Spiglanin, Saturation kinetics of the S 0 to S 2 optical transition in isolated diphenylhexatriene, The Journal of Chemical Physics 82, 2939 (1985).
- [56] A. Chaieb, A. Khoukh, R. Brown, J. François, and C. Dagron-Lartigau, Characterization of model luminescent PPV analogues with donating or withdrawing groups, Optical Materials 30, 318 (2007).
- [57] F. A. Cotton, Chemical applications of group theory, 3rd ed. (J. Wiley & sons, New York Chichester Brisbane [etc.], 1990).
- [58] R. R. Birge, M. Z. Zgierski, L. Serrano-Andres, and B. S. Hudson, Transition dipole orientation of linear polyenes: Semiempirical models and extrapolation to the infinite chain limit, The Journal of Physical Chemistry A 103, 2251 (1999).
- [59] K. Aidas, C. Angeli, K. L. Bak, V. Bakken, R. Bast, L. Boman, O. Christiansen, R. Cimiraglia, S. Coriani, P. Dahle, E. K. Dalskov, U. Ekström, T. Enevoldsen, J. J. Eriksen, P. Ettenhuber, B. Fernández, L. Ferrighi, H. Fliegl, L. Frediani, K. Hald, A. Halkier, C. Hättig, H. Heiberg, T. Helgaker, A. C. Hennum, H. Hettema, E. Hjertenæs, S. Høst, I. Høyvik, M. F. Iozzi, B. Jansík, H. J. A. Jensen, D. Jonsson, P. Jørgensen, J. Kauczor, S. Kirpekar, T. Kjærgaard, W. Klopper, S. Knecht, R. Kobayashi, H. Koch, J. Kongsted, A. Krapp, K. Kristensen, A. Ligabue, O. B. Lutnæs, J. I. Melo, K. V. Mikkelsen, R. H. Myhre, C. Neiss, C. B. Nielsen, P. Norman, J. Olsen, J. M. H. Olsen, A. Osted, M. J. Packer,

- F. Pawlowski, T. B. Pedersen, P. F. Provasi, S. Reine, Z. Rinkevicius, T. A. Ruden, K. Ruud, V. V. Rybkin, P. Sałek, C. C. M. Samson, A. S. De Merás, T. Saue, S. P. A. Sauer, B. Schimmelpfennig, K. Sneskov, A. H. Steindal, K. O. Sylvester-Hvid, P. R. Taylor, A. M. Teale, E. I. Tellgren, D. P. Tew, A. J. Thorvaldsen, L. Thøgersen, O. Vahtras, M. A. Watson, D. J. D. Wilson, M. Ziolkowski, and H. Ågren, enThe Dalton quantum chemistry program system, WIREs Computational Molecular Science 4, 269 (2014).
- [60] Dalton, a molecular electronic structure program, Release v2020.1 (2022), http://daltonprogram.org.
- [61] B. M. Wong and T. H. Hsieh, Optoelectronic and excitonic properties of oligoacenes: Substantial improvements from range-separated time-dependent density functional theory, Journal of Chemical Theory and Computation 6, 3704 (2010).
- [62] I. A. Elayan, L. Rib, R. A. Mendes, and A. Brown, Beyond explored functionals: A computational journey of two-photon absorption, Journal of Chemical Theory and Computation 20, 3879 (2024).
- [63] M. B. Oviedo, N. V. Ilawe, and B. M. Wong, Polarizabilities of -conjugated chains revisited: Improved results from broken-symmetry range-separated DFT and new CCSD(T) benchmarks, Journal of Chemical Theory and Computation 12, 3593 (2016).
- [64] M. J. Frisch, G. W. Trucks, H. B. Schlegel, G. E. Scuseria, M. A. Robb, J. R. Cheeseman, G. Scalmani, V. Barone, G. A. Petersson, H. Nakatsuji, X. Li, M. Caricato, A. V. Marenich, J. Bloino, B. G. Janesko, R. Gomperts, B. Mennucci, H. P. Hratchian, J. V. Ortiz, A. F. Izmaylov, J. L. Sonnenberg, D. Williams-Young, F. Ding, F. Lipparini, F. Egidi, J. Goings, B. Peng, A. Petrone, T. Henderson, D. Ranasinghe, V. G. Zakrzewski, J. Gao, N. Rega, G. Zheng, W. Liang, M. Hada, M. Ehara, K. Tovota, R. Fukuda, J. Hasegawa, M. Ishida, T. Nakajima, Y. Honda, O. Kitao, H. Nakai, T. Vreven, K. Throssell, J. A. Montgomery, Jr., J. E. Peralta, F. Ogliaro, M. J. Bearpark, J. J. Heyd, E. N. Brothers, K. N. Kudin, V. N. Staroverov, T. A. Keith, R. Kobayashi, J. Normand, K. Raghavachari, A. P. Rendell, J. C. Burant, S. S. Iyengar, J. Tomasi, M. Cossi, J. M. Millam, M. Klene, C. Adamo, R. Cammi, J. W. Ochterski, R. L. Martin, K. Morokuma, O. Farkas, J. B. Foresman, and D. J. Fox, Gaussian 16 Revision C.01 (2016), gaussian Inc. Wallingford CT.
- [65] R. L. Christensen, M. G. I. Galinato, E. F. Chu, J. N. Howard, R. D. Broene, and H. A. Frank, Energies of lowlying excited states of linear polyenes, The Journal of Physical Chemistry A 112, 12629 (2008).
- [66] C. Sutton, Y. Yang, D. Zhang, and W. Yang, Single, double electronic excitations and exciton effective conjugation lengths in π-conjugated systems, The Journal of Physical Chemistry Letters 9, 4029 (2018).
- [67] C. Naim, R. Zaleśny, and D. Jacquemin, Two-photon absorption strengths of small- and medium-sized molecules: Reference cc3 values and benchmarks (2024).
- [68] A. Dreuw and M. Head-Gordon, Single-reference ab initio methods for the calculation of excited states of large molecules, Chemical reviews 105, 4009 (2005).
- [69] V. P. Gupta, Principles and applications of quantum chemistry (Academic Press is an imprint of Elsevier, London, UK, 2016).
- [70] M. C. Zerner, G. H. Loew, R. F. Kirchner, and U. T.

- Mueller-Westerhoff, An intermediate neglect of differential overlap technique for spectroscopy of transition-metal complexes. Ferrocene, Journal of the American Chemical Society 102, 589 (1980).
- [71] B. De Nijs, R. W. Bowman, L. O. Herrmann, F. Benz, S. J. Barrow, J. Mertens, D. O. Sigle, R. Chikkaraddy, A. Eiden, A. Ferrari, O. A. Scherman, and J. J. Baumberg, Unfolding the contents of sub-nm plasmonic gaps using normalising plasmon resonance spectroscopy, Faraday Discussions 178, 185 (2015).
- [72] J. J. Baumberg, J. Aizpurua, M. H. Mikkelsen, and D. R. Smith, Extreme nanophotonics from ultrathin metallic gaps, Nature Materials 18, 668 (2019).
- [73] COMSOL Multiphysics® v. 6.3., www.comsol.com.

- COMSOL AB, Stockholm, Sweden.
- [74] S. Thomas, G. Wachter, C. Lemell, J. Burgdörfer, and P. Hommelhoff, Large optical field enhancement for nanotips with large opening angles, New Journal of Physics 17, 063010 (2015), publisher: IOP Publishing.
- [75] J. Ma, J. Zhang, J. Horder, A. A. Sukhorukov, M. Toth, D. N. Neshev, and I. Aharonovich, Engineering Quantum Light Sources with Flat Optics, Advanced Materials 36, 10.1002/adma.202313589 (2024), publisher: Wiley.
- [76] A. Orieux, M. A. M. Versteegh, K. D. Jöns, and S. Ducci, Semiconductor devices for entangled photon pair generation: a review, Reports on Progress in Physics 80, 076001 (2017), publisher: IOP Publishing.